

See discussions, stats, and author profiles for this publication at: <https://www.researchgate.net/publication/238654010>

# IRAS studies of NO<sub>2</sub>, N<sub>2</sub>O<sub>3</sub>, and N<sub>2</sub>O<sub>4</sub> adsorbed on Au(111) surfaces and reactions with coadsorbed H<sub>2</sub>O

ARTICLE *in* THE JOURNAL OF PHYSICAL CHEMISTRY A · OCTOBER 1998

Impact Factor: 2.69 · DOI: 10.1021/jp982061d

---

CITATIONS

81

---

READS

64

2 AUTHORS, INCLUDING:



Bruce Koel

Princeton University

296 PUBLICATIONS 8,975 CITATIONS

SEE PROFILE

# IRAS Studies of NO<sub>2</sub>, N<sub>2</sub>O<sub>3</sub>, and N<sub>2</sub>O<sub>4</sub> Adsorbed on Au(111) Surfaces and Reactions with Coadsorbed H<sub>2</sub>O

Jiang Wang and Bruce E. Koel\*

Department of Chemistry, University of Southern California, Los Angeles, California 90089-0482

Received: April 29, 1998; In Final Form: August 18, 1998

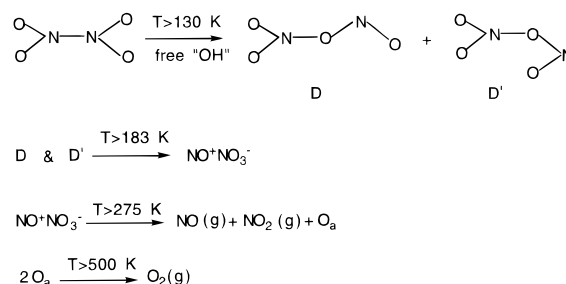
Adsorption or bonding geometries of pure adlayers of several N<sub>x</sub>O<sub>y</sub> species, i.e., nitrogen dioxide (NO<sub>2</sub>), dinitrogen trioxide (N<sub>2</sub>O<sub>3</sub>), and dinitrogen tetroxide (N<sub>2</sub>O<sub>4</sub>), on Au(111) were determined by utilizing infrared reflection–absorption spectroscopy (IRAS). Dosing NO<sub>2</sub> on Au(111) at 85 K produced, in our experiments, mixtures of NO<sub>2</sub> and N<sub>2</sub>O<sub>3</sub> (from contaminant NO) at submonolayer coverages and NO<sub>2</sub>, N<sub>2</sub>O<sub>3</sub>, and N<sub>2</sub>O<sub>4</sub> at monolayer coverages. However, a pure adlayer of chemisorbed NO<sub>2</sub> could be prepared by forming the monolayer on Au(111) at 85 K and then heating to 185 K or by NO<sub>2</sub> exposures on Au(111) at 185 K. Chemisorbed NO<sub>2</sub> is bonded to the surface in an O,O'-chelating geometry with C<sub>2v</sub> symmetry. A monolayer of adsorbed N<sub>2</sub>O<sub>3</sub> was produced by exposing the pure, chelating NO<sub>2</sub> adlayer to NO(g). The adsorbed complex with N<sub>2</sub>O<sub>3</sub> has C<sub>s</sub> symmetry, and we believe that N<sub>2</sub>O<sub>3</sub> is bonded to the surface through one oxygen. Large NO<sub>2</sub> exposures can be used to produce crystalline N<sub>2</sub>O<sub>4</sub> multilayers that have a preferential orientation of the N–N bond perpendicular to the Au(111) surface. To probe important aspects of the reactivity of these species with water and to investigate structure–reactivity relationships in this chemistry, we studied the reaction of each of these species with coadsorbed H<sub>2</sub>O. Upon being heated, reactions proceed via two pathways. One route produces nitrous acid (HONO) and nitric acid (HNO<sub>3</sub>) and occurs for all of the nitrogen oxide species listed above. These reactions do not depend on the degree of crystallinity of the condensed water clusters. A separate path occurs only for co-condensed amorphous ice clusters and multilayer N<sub>2</sub>O<sub>4</sub> films, as signaled by the formation of oxygen adatoms on the Au(111) surface. These results reveal new information about fundamental interactions of nitrogen oxides and water in condensed phases.

## 1. Introduction

Nitrogen oxides exhibit a wide variety of structures and have a rich chemistry.<sup>1</sup> Also, many different metastable N<sub>x</sub>O<sub>y</sub> intermediates<sup>2</sup> can be formed during reactions, and taken together, this has limited the understanding of the chemistry of nitrogen oxides and the development of structure–reactivity relationships. In particular, for interactions with metal atoms, a variety of bonding geometries are usually available. For example, NO<sub>2</sub> is well-known as a versatile linkage isomer in coordination compounds<sup>3</sup> and on metal surfaces.<sup>4,5</sup> However, we believe that it is possible to exploit this versatility to cleanly prepare and probe the condensed-phase chemistry of NO<sub>2</sub> and other nitrogen oxides by utilizing suitable substrates in surface-science-type experiments.

Au(111) surfaces are very unreactive and thus can be used in many cases to serve as an inert support for condensed phases. Recently, we have studied reactions after NO<sub>2</sub> exposures on ice films on Au(111).<sup>6,7</sup> We proposed that two separate reaction channels occur. One pathway forms nitrous acid (HONO) and nitric acid (HNO<sub>3</sub>) and occurs for reactions of either amorphous or crystalline ice with NO<sub>2</sub>, N<sub>2</sub>O<sub>3</sub>, and N<sub>2</sub>O<sub>4</sub> at temperatures below 145 K. Another pathway ultimately forms oxygen adatoms on the Au(111) surface. In these reactions, we believe that Au(111) does not play a significant role in the nascent chemistry of H<sub>2</sub>O + NO<sub>2</sub> but rather serves as an integrating detector for certain reaction products by decomposing those

products at higher temperatures to produce surface oxygen. In this latter reaction channel, we observed two intermediates, the nitrito isomer of N<sub>2</sub>O<sub>4</sub> (ONO–NO<sub>2</sub>) and nitrosonium nitrate (NO<sup>+</sup>NO<sub>3</sub><sup>−</sup>), and we proposed that N<sub>2</sub>O<sub>4</sub> was responsible for the formation of oxygen adatoms as shown in the following mechanism.<sup>7</sup>



In these reactions, however, the specific reactivity of NO<sub>2</sub> or N<sub>2</sub>O<sub>3</sub> with ice and their role in oxygen formation remains unclear. Use of a Au(111) substrate also allows us to address these issues. Previously, we have studied NO<sub>2</sub> adsorption on Au(111)<sup>8</sup> and Au(poly)<sup>9</sup> by HREELS and TPD and proposed methods to produce pure NO<sub>2</sub> and N<sub>2</sub>O<sub>3</sub> monolayers on Au surfaces. Because we can separately form pure NO<sub>2</sub> and N<sub>2</sub>O<sub>3</sub> monolayers on Au(111), we can better understand the individual reactivities of NO<sub>2</sub> and N<sub>2</sub>O<sub>3</sub> with H<sub>2</sub>O, as either amorphous or crystalline ice, by preadsorbing pure NO<sub>2</sub> and N<sub>2</sub>O<sub>3</sub> monolayers on Au(111) and studying the subsequent surface reactions with postdosed water to form ice films.

\* To whom correspondence should be addressed.

This paper presents results of temperature-programmed desorption (TPD) and infrared reflection–absorption spectroscopy (IRAS) investigations of the composition and adsorption geometry of  $\text{NO}_2$ ,  $\text{N}_2\text{O}_3$ , and  $\text{N}_2\text{O}_4$  adlayers on Au(111). We also obtain new information on the reacting species in condensed films of  $\text{NO}_2 + \text{H}_2\text{O}$  that lead to oxygen formation on the Au(111) surface. Pure  $\text{N}_2\text{O}_3$  and chemisorbed, chelating  $\text{NO}_2$  monolayers do not react with amorphous ice to form oxygen on Au(111). Only  $\text{N}_2\text{O}_4$  multilayer films produce oxygen adatoms in these reactions, and the results are identical to those obtained by reacting  $\text{N}_2\text{O}_4$  films on ice films pre-formed on the Au(111) surface. This further supports our proposal that formation of the nascent intermediates that lead to oxygen deposition on the Au(111) surface is not caused by the presence of the Au surface atoms but is caused by “free OH” groups on the amorphous ice surface.

## 2. Experimental Methods

The stainless steel ultra-high vacuum (UHV) chamber used in these experiments was pumped by a 240 L/s ion pump, a 240 L/s turbomolecular pump, and a titanium sublimation pump. The base pressure was typically  $2 \times 10^{-10}$  Torr. The UHV chamber was equipped with a double-pass cylindrical mirror analyzer (CMA) for Auger electron spectroscopy (AES), reverse-view four-grid optics for low-energy electron diffraction (LEED), a UTI 100 C quadrupole mass spectrometer (QMS) for temperature-programmed desorption (TPD), and gas-dosing facilities.

Infrared reflection–absorption spectroscopy (IRAS) studies were carried out in a reaction antechamber attached to the top of the surface analysis chamber by using a Mattson Galaxy 6020 FTIR spectrometer.  $\text{Ar}^+$  ion sputtering was also performed in this antechamber. The IR beam from the interferometer was focused on the crystal at a grazing incidence angle of  $\sim 86^\circ$ . The reflected light along the specular direction was recollimated and focused onto a narrow-band, liquid nitrogen-cooled mercury cadmium telluride (MCT) detector. IR spectra were collected with the sample at 86 K using  $8\text{ cm}^{-1}$  resolution and 1000 scans in a 4 min. period. Clean surface (background) spectra were acquired after annealing the crystal to 550 K to desorb adsorbates and quickly cooling to 86 K, and these were then subtracted from the adsorbate-covered surface spectra.

TPD experiments were carried out using a random flux shield over the end of the QMS, with the sample approximately 0.5 cm away from the entrance aperture and in the line-of-sight of the QMS ionizer. Two high-transparency screens, one biased at  $-55\text{ V}$  on the end of the ionizer cage and one at ground potential on the flux shield, were used to suppress the low-energy electron flux from the QMS.<sup>10</sup> The heating rate in TPD was 3.5 K/s.

The Au(111) crystal was mounted as reported before.<sup>6,7</sup> The sample could be cooled to 85 K using liquid nitrogen or resistively heated to 1100 K. The temperature was measured by a chromel–alumel thermocouple pressed firmly into a hole drilled into the side of the crystal. The Au(111) surface was cleaned by repeated sputtering–annealing cycles using 500 eV  $\text{Ar}^+$  bombardment at 300 K followed by annealing to 973 K for 10 min. The cleanliness and structure of the surface were checked by AES and LEED.

$\text{NO}$ ,  $\text{NO}_2$ , and  $\text{H}_2\text{O}$  exposures were made by means of a directed molecular beam doser utilizing a microcapillary array.  $\text{NO}$  (Matheson, 99.9%) and  $\text{NO}_2$  (Matheson, 99.9%) were used as received. Deionized water ( $\text{H}_2\text{O}$ ) was used after degassing

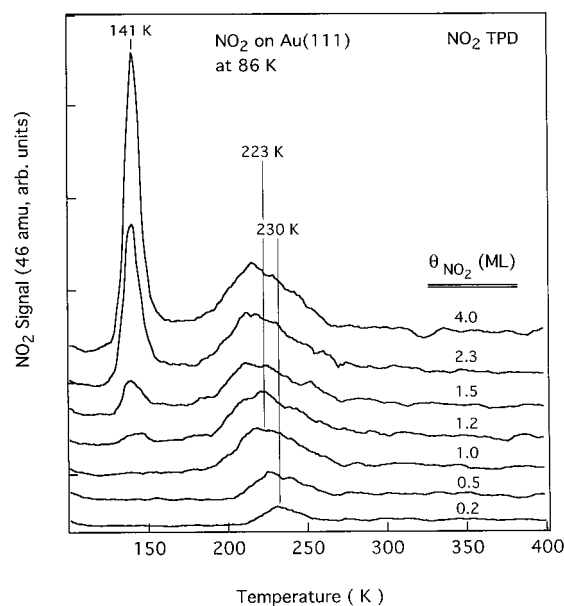


**Figure 1.**  $\text{NO}_2$  TPD spectra following  $\text{NO}_2$  exposures on Au(111) at 86 K.

via several freeze–pump–thaw cycles. To minimize reactions of  $\text{NO}_2$  in the doser gas lines, stainless steel and gold-plated gaskets were utilized and the entire dosing manifold gas line was initially passivated at  $\sim 150^\circ\text{C}$  under  $\text{NO}_2$  pressure for 30 min.

Adsorbate coverages herein are referenced to  $\Theta = 1\text{ ML}$  for the saturation monolayer coverage of a given adsorbate on the Au(111) surface.  $\text{NO}_2$  monolayer coverages were determined by TPD, referenced to saturation of the chemisorbed  $\text{NO}_2$  peak at 220 K, which was defined as  $\Theta_{\text{NO}_2} = 1\text{ ML}$  (or  $4.2 \times 10^{14}$  molecules/ $\text{cm}^2$ ).<sup>8</sup> The  $\text{H}_2\text{O}$  monolayer coverage was much less certain and was difficult to establish. Briefly, we used a background gas dose sufficient to adsorb one-half of the molecules required for the water bilayer ( $1.0 \times 10^{15}$  molecules/ $\text{cm}^2$ ) found on Pt(111)<sup>11</sup> assuming unit sticking probability.

## 3. Results and Discussion

**3.1. Formation of Pure  $\text{NO}_2$ ,  $\text{N}_2\text{O}_3$ , and  $\text{N}_2\text{O}_4$  Adlayers on Au(111).** Figure 1 shows TPD spectra for  $\text{NO}_2$  desorption following  $\text{NO}_2$  exposures on Au(111) at 86 K.  $\text{NO}_2$  desorption initially occurs in a peak that shifts from 230 to 217 K with increasing coverage and then in a low-temperature peak at 141 K at higher exposures. This is consistent with earlier studies of  $\text{NO}_2/\text{Au}(111)$  that found completely reversible adsorption and assigned a peak at 223 K to desorption from the chemisorbed monolayer and a peak at 141 K to desorption from physisorbed  $\text{N}_2\text{O}_4$  multilayers.<sup>8,9,12</sup> In Figure 1, we do not see any desorption at 325 K, which is an important feature in  $\text{NO}_2$  TPD from Au-(poly) surfaces,<sup>9</sup> indicating that our crystal had a negligible number of defects. The desorption activation energy for chemisorbed  $\text{NO}_2$  was previously estimated to be 58 kJ/mol, and that for  $\text{N}_2\text{O}_4$  multilayers was estimated to be 35 kJ/mol.<sup>8</sup>

Chemisorbed  $\text{NO}_2$  on Au(111) has been assigned as an O,O'-nitrito surface chelate with  $\text{C}_{2v}$  symmetry based on HREELS.<sup>8</sup> Often, however, when working with HREELS resolutions of  $80\text{ cm}^{-1}$  or so, there is a chance that overlapping peaks are not resolved and there is a small possibility that the loss peak at  $1180\text{ cm}^{-1}$  in the work cited above could be due to two peaks of nearly the same energy arising from the asymmetric  $\nu_a(\text{NO}_2)$  and symmetric  $\nu_s(\text{NO}_2)$   $\text{NO}_2$  stretching modes. Interaction with the Au(111) surface could markedly decrease the energies of

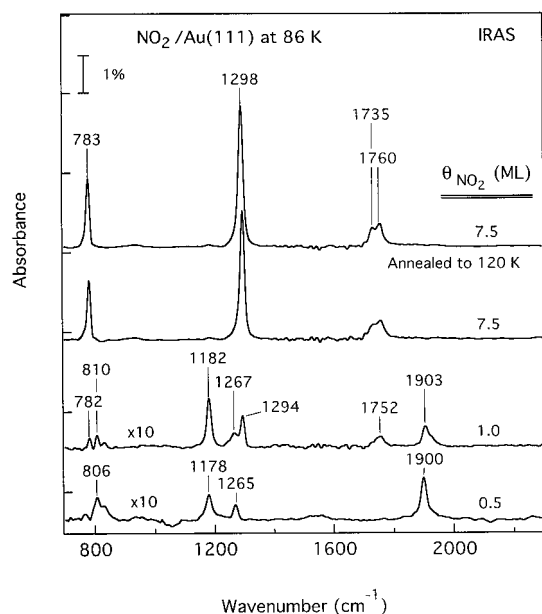


**Figure 2.** IRAS spectra after NO<sub>2</sub> exposures on a Au(111) surface at 86 K. All of the spectra were collected at 86 K.

both of the  $\nu_a(\text{NO}_2)$  and  $\nu_s(\text{NO}_2)$  modes, which are 1618 and 1318 cm<sup>-1</sup>, respectively in the NO<sub>2</sub> gas-phase IR spectrum.<sup>13</sup> For example, the NO<sub>2</sub> group in Ni( $\alpha$ -picoline)<sub>2</sub>(NO<sub>2</sub>)<sub>2</sub><sup>14</sup> has  $\Delta[\nu_a(\text{NO}_2) - \nu_s(\text{NO}_2)] = 73$  cm<sup>-1</sup>.

To better elucidate the adlayer composition and bonding geometry with increasing coverage and film thickness, we have obtained IRAS spectra of the adsorbed layers following NO<sub>2</sub> exposures on Au(111) at 86 K, as shown in Figure 2. Our assignments of these spectra are given in Table 1, and these agree with our previous HREELS data<sup>8</sup> very well. At 0.5 ML NO<sub>2</sub> coverage, a mixture of chemisorbed NO<sub>2</sub> and N<sub>2</sub>O<sub>3</sub> exists on Au(111). N<sub>2</sub>O<sub>3</sub> is formed by reaction of chemisorbed NO<sub>2</sub> with residual NO<sup>8</sup> in the background that arises from decomposition of NO<sub>2</sub> in the UHV chamber. Chemisorbed NO<sub>2</sub> has two peaks at 1178 and 806 cm<sup>-1</sup> assigned previously to the symmetric stretching,  $\nu_s(\text{NO}_2)$ , and symmetric bending,  $\delta(\text{NO}_2)$ , modes, respectively, for a species bonded in an upright O,O'-chelating geometry with C<sub>2v</sub> symmetry.<sup>8</sup> Two peaks due to N<sub>2</sub>O<sub>3</sub> are seen at 1900 and 1265 cm<sup>-1</sup> that arise from NO stretching,  $\nu(\text{NO})$ , and NO<sub>2</sub> asymmetric stretching,  $\nu_a(\text{NO}_2)$ , modes, respectively. The other two peaks from N<sub>2</sub>O<sub>3</sub> appear at 1178 and 806 cm<sup>-1</sup> due to the  $\nu_s(\text{NO}_2)$  and  $\delta(\text{NO}_2)$  modes, which overlap with the same modes of chelating NO<sub>2</sub>. At 1 ML NO<sub>2</sub> coverage, the adsorbed species are chelating NO<sub>2</sub>, N<sub>2</sub>O<sub>3</sub>, and N<sub>2</sub>O<sub>4</sub>. The peaks at 1182 and 810 cm<sup>-1</sup> are due to chemisorbed chelating NO<sub>2</sub>. The peaks at 1903, 1267, 1182, and 810 cm<sup>-1</sup> are from N<sub>2</sub>O<sub>3</sub>. The peaks at 1760, 1735, 1294, and 783 cm<sup>-1</sup> are due to the  $\nu_a(\text{NO}_2)$ ,  $\nu_s(\text{NO}_2)$ , and  $\delta(\text{NO}_2)$  modes, respectively, of N<sub>2</sub>O<sub>4</sub>.<sup>7,8,15,16</sup> When the NO<sub>2</sub> coverage is 7.5 ML, only bands due to N<sub>2</sub>O<sub>4</sub> were observed. Annealing

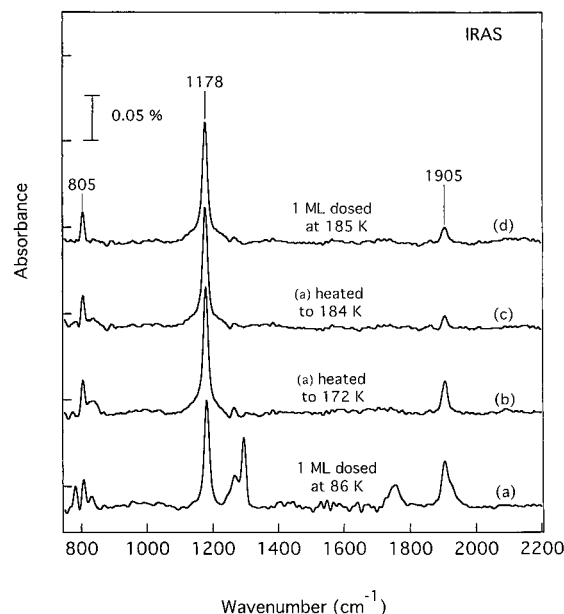


**Figure 3.** IRAS spectra obtained following: (a) 1 ML NO<sub>2</sub> dosed on Au(111) at 86 K; (b) annealing the surface in (a) to 172 K for 30 s; (c) annealing the surface in (a) to 184 K for 30 s; (d) dosing 1 ML NO<sub>2</sub> at 185 K. All of the spectra were collected at 86 K.

this multilayer to 120 K does not change the IRAS spectra. This multilayer film can be described as pure crystalline N<sub>2</sub>O<sub>4</sub> with a preferential orientation of the N—N bond almost perpendicular to the Au(111) surface, since it shows strong peaks due to  $\nu_s(\text{NO}_2)$  modes along with fairly weak peaks due to  $\nu_a(\text{NO}_2)$  modes.<sup>15,16</sup>

While the top two spectra in Figure 2 nicely characterize a condensed film with a pure N<sub>2</sub>O<sub>4</sub> surface layer, we also wanted to obtain pure NO<sub>2</sub> and N<sub>2</sub>O<sub>3</sub> layers. These were made by the procedure outlined in Bartram et al.,<sup>8</sup> and our IRAS spectra for chemisorbed NO<sub>2</sub> are shown in Figure 3. The pure, chemisorbed monolayer of NO<sub>2</sub> can be made by dosing NO<sub>2</sub> on Au(111) at 185 K or by dosing a NO<sub>2</sub> monolayer at 86 K and then heating to 185 K. Peaks at 1179 and 804 cm<sup>-1</sup> are characteristic for chelating NO<sub>2</sub><sup>-</sup> ligands in transition metal compounds.<sup>3</sup> As we have discussed for these compounds in more detail previously,<sup>8</sup> the  $\delta(\text{NO}_2)$  mode is typically insensitive to the bonding geometry of NO<sub>2</sub>, occurring at 817–863 cm<sup>-1</sup>, but the  $\nu_s(\text{NO}_2)$  mode is very sensitive to this bonding geometry. The  $\nu_s(\text{NO}_2)$  mode has a frequency of 1171–1225 cm<sup>-1</sup> for chelating isomers and 1306–1392 cm<sup>-1</sup> for nitro isomers.<sup>3,14,17</sup> IRAS detects only one peak in the 1120–1220 cm<sup>-1</sup> range that must be due to  $\nu_s(\text{NO}_2)$  and no feature that can be assigned to  $\nu_a(\text{NO}_2)$ . Therefore, because of the strict dipole selection rule in IRAS (compared to HREELS) we show conclusively that chemisorbed NO<sub>2</sub> is bonded in an O,O'-chelating geometry with C<sub>2v</sub> symmetry on Au(111), confirming the previous assignment made by using HREELS. The small peak at 1903 cm<sup>-1</sup> is due

**TABLE 1: Vibrational Frequencies (cm<sup>-1</sup>) and Assignments of Adsorbed NO<sub>2</sub>, N<sub>2</sub>O<sub>3</sub>, and N<sub>2</sub>O<sub>4</sub> on Au(111) Surfaces**

mode	NO <sub>2</sub> /Au(111) NO <sub>2</sub> monolayer		N <sub>2</sub> O <sub>3</sub> /Au(111) N <sub>2</sub> O <sub>3</sub> monolayer		N <sub>2</sub> O <sub>4</sub> /Au(111) N <sub>2</sub> O <sub>4</sub> multilayer		
	HREELS <sup>8</sup>	IRAS	HREELS <sup>8</sup>	IRAS	HREELS <sup>8</sup>	IRAS <sup>16</sup>	IRAS
$\nu(\text{O}_2\text{N}-\text{NO})$			250				
$\rho(\text{O}_2\text{NNO})$			450–650		440		
$\delta_s(\text{NO}_2)$	800	805	800	806	770	785	783
$\nu_s(\text{NO}_2)$	1180	1178	1180	1182	1280	1301	1298
$\nu_a(\text{NO}_2)$	1180		1270	1272	1755	1750	1735, 1760
$\nu(\text{NO})$			1890	1897			

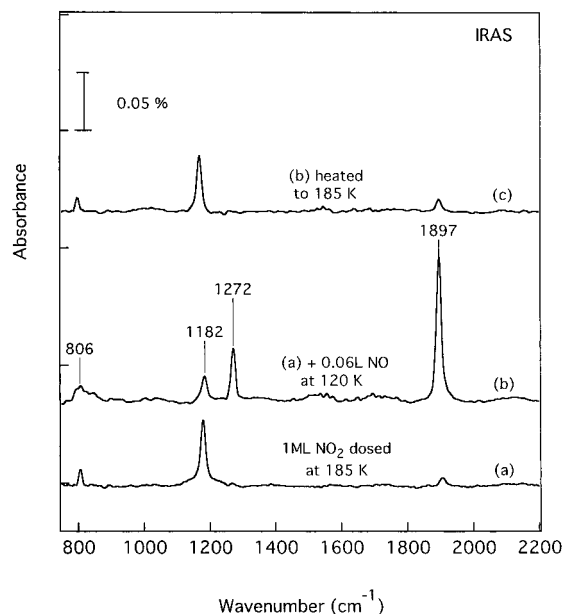


**Figure 4.** IRAS spectra obtained after (a) 1 ML  $\text{NO}_2$  dosed on Au(111) at 185 K to give a pure monolayer of chelating chemisorbed  $\text{NO}_2$ , (b) NO exposure on a Au(111) surface precovered by the chelating  $\text{NO}_2$  monolayer at 120 K to form a pure  $\text{N}_2\text{O}_3$  monolayer, and (c) annealing the surface in (b) to 185 K for 30 s. All of the spectra were collected at 86 K.

to the formation of a very small amount of  $\text{N}_2\text{O}_3$  by reaction of residual NO in the chamber with chemisorbed  $\text{NO}_2$ .

A pure  $\text{N}_2\text{O}_3$  monolayer can be readily made from the pure chelating  $\text{NO}_2$  monolayer on Au(111) by NO exposure to the adlayer at 120 K. All of the peaks in the IRAS spectrum in Figure 4 can be assigned to  $\text{N}_2\text{O}_3$ . The strongest peak at 1898  $\text{cm}^{-1}$  is due to the  $\nu(\text{N}=\text{O})$  mode, and the peaks at 1273, 1184, and 804  $\text{cm}^{-1}$  are due to the  $\nu_a(\text{NO}_2)$ ,  $\nu_s(\text{NO}_2)$ , and  $\delta(\text{NO}_2)$  modes, respectively. We propose that adsorbed  $\text{N}_2\text{O}_3$  is bonded to the surface with  $C_s$  symmetry using one oxygen atom, in a monodentate fashion, with its  $\text{O}_2\text{NN}=\text{O}$  bond perpendicular to the Au(111) surface. First, the  $\nu_a(\text{NO}_2)$  and  $\nu_s(\text{NO}_2)$  peaks have comparable intensity in the gas phase, and we observed comparable intensity of the  $\nu_a(\text{NO}_2)$  and  $\nu_s(\text{NO}_2)$  modes for the chemisorbed species. The surface dipole selection rule should strongly attenuate the  $\nu_a(\text{NO}_2)$  peak if a chelating  $\text{O}, \text{O}'$ -geometry were formed, and this does not occur. The observation of IR intensity ratios of the other bands different from those in gas-phase  $\text{N}_2\text{O}_3$ <sup>18</sup> indicates that the adsorbed species is oriented and that this orientation is not with the molecular plane parallel with the surface. Furthermore, the very strong intensity of the  $\nu(\text{N}=\text{O})$  mode is consistent with this dynamic dipole nearly perpendicular to the surface. When this monodentate  $\text{N}_2\text{O}_3$  adlayer is heated to 185 K, chelating  $\text{NO}_2$  appears again on the surface following the breaking of the N–N bond in  $\text{N}_2\text{O}_3$ . This is consistent with an N–N bond dissociation energy of 42 kJ/mol.<sup>8</sup> We can now point out that the strong  $\nu(\text{N}=\text{O})$  peak of pure adsorbed  $\text{N}_2\text{O}_3$  shows that the amount of  $\text{N}_2\text{O}_3$  coadsorbed with chelating  $\text{NO}_2$  in Figure 3 is very small indeed.

Since NO is not adsorbed on the Au(111) surface even at 105 K,<sup>8</sup> this reaction likely occurs via an Eley–Rideal mechanism.<sup>19</sup> Chelating  $\text{NO}_2$  on the Au(111) surface may exist as a surface-bound radical, with an unpaired electron on the N atom (if the hybridization of the gas-phase molecule is maintained), and the radical–radical coupling reaction with NO (also a radical with the unpaired electron on the N atom) would readily occur. The following schematic illustrates the proposed bidentate  $\text{NO}_2$  and monodentate  $\text{N}_2\text{O}_3$  species formed on Au(111).

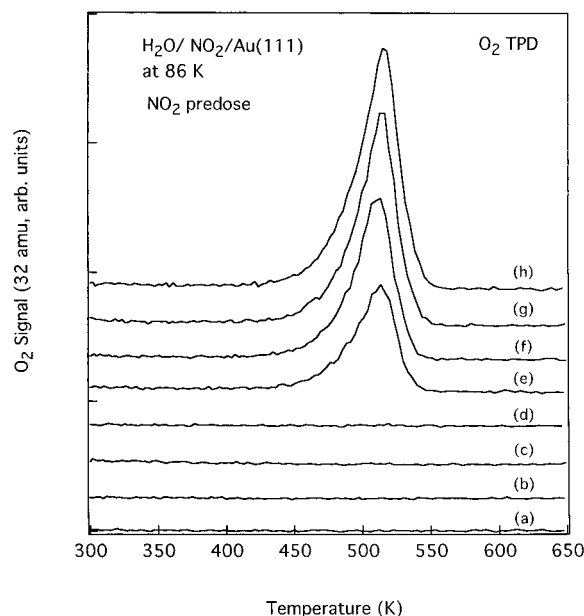
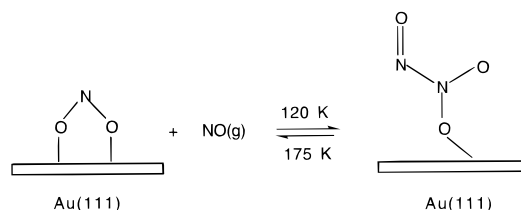


**Figure 5.**  $\text{O}_2$  TPD spectra after predosing  $\text{NO}_2$  on Au(111) at 86 K followed by  $\text{H}_2\text{O}$  exposures at the same temperature: (a) 1 ML  $\text{H}_2\text{O}$  dose after 0.5 ML  $\text{NO}_2$ ; (b) 6 ML  $\text{H}_2\text{O}$  dose after 0.5 ML  $\text{NO}_2$ ; (c) 0.5 ML  $\text{H}_2\text{O}$  dose after 1 ML  $\text{NO}_2$ ; (d) 6 ML  $\text{H}_2\text{O}$  dose after 1 ML  $\text{NO}_2$ ; (e) 1 ML  $\text{H}_2\text{O}$  dose after 5 ML  $\text{NO}_2$ ; (f) 1 ML  $\text{H}_2\text{O}$  dose after 7.5 ML  $\text{NO}_2$ ; (g) 4.5 ML  $\text{H}_2\text{O}$  dose after 7.5 ML  $\text{NO}_2$ ; (h) 4.5 ML  $\text{H}_2\text{O}$  dose after 10 ML  $\text{NO}_2$ .



In all these IRAS studies, we did not observe any evidence for nitrite– $\text{N}_2\text{O}_4$  or  $\text{NO}^+\text{NO}_3^-$  species formed from  $\text{NO}_2$  exposures on Au(111). Koch et al.<sup>16</sup> did not observe these species either when they studied  $\text{NO}_2$  adsorption on gold foil at 80 K.

**3.2. Reactions of  $\text{H}_2\text{O}$  with Predesorbed  $\text{NO}_2$ ,  $\text{N}_2\text{O}_3$ , and  $\text{N}_2\text{O}_4$  on Au(111).** Water interacts very weakly with the Au(111) surface, TPD of  $\text{H}_2\text{O}$  on Au(111) does not resolve the desorption of any strongly bound, chemisorbed state, and no decomposition occurs.<sup>7,20</sup> Consistent with these reports, our TPD spectra show only a single narrow  $\text{H}_2\text{O}$  desorption peak, ranging from 153 to 165 K as the coverage increases.

Although  $\text{NO}_2$  and  $\text{H}_2\text{O}$  adsorb molecularly and reversibly when adsorbed separately, coadsorption leads to reactions. Those reactions that lead ultimately to the deposition of oxygen adatoms on the surface are the easiest to monitor, because oxygen adatoms recombine on Au(111) and desorb as  $\text{O}_2$  at 520–545 K leaving a clean surface.<sup>21,22</sup> Figure 5 shows  $\text{O}_2$  TPD spectra that we used to monitor these reactions for a variety of coadsorption conditions. All of the exposures of both  $\text{H}_2\text{O}$  and  $\text{NO}_2$  were carried out with the crystal at 86 K. The deposition of amorphous ice occurs at this low surface temperature.<sup>7,23,24</sup>  $\text{O}_2$  desorption only results when the  $\text{NO}_2$  preexposure was in the multilayer range forming a pure  $\text{N}_2\text{O}_4$  film. The amount of oxygen formation saturates for  $\text{NO}_2$  preexposures exceeding 10 ML. For  $\text{NO}_2$  preexposures in the submonolayer range, forming a  $\text{NO}_2$  and  $\text{N}_2\text{O}_3$  precovered Au(111) surface, parts a and b of Figure 5 show that no oxygen was produced



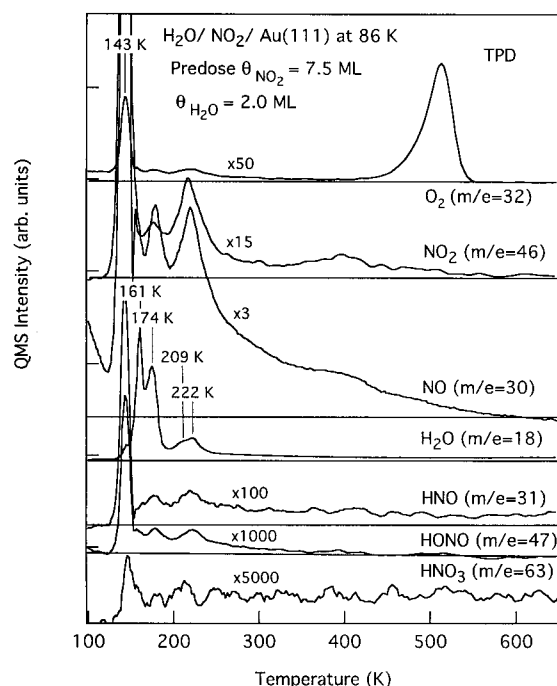


**Figure 6.** TPD spectra for several detected gas-phase products formed during heating in TPD after predosing 7.5 ML NO<sub>2</sub> on Au(111) at 86 K followed by a 2 ML H<sub>2</sub>O exposure at the same temperature.

for 1–6 ML H<sub>2</sub>O postdoses. This indicates that NO<sub>2</sub> and N<sub>2</sub>O<sub>3</sub> are not responsible for oxygen formation. Moreover, parts c and d of Figure 5 show that no oxygen is produced when different postexposures of H<sub>2</sub>O were dosed on the adlayer formed from a 1 ML NO<sub>2</sub> exposure on Au(111). This NO<sub>2</sub> dose forms a mixture of NO<sub>2</sub>, N<sub>2</sub>O<sub>3</sub>, and N<sub>2</sub>O<sub>4</sub> covering the surface. This result implies that interactions (hydrogen bonding) between N<sub>2</sub>O<sub>4</sub> clusters and amorphous ice clusters are critical for oxygen deposition and coadsorbed NO<sub>2</sub> and N<sub>2</sub>O<sub>3</sub> can block this interaction. These results are consistent with our observations that only N<sub>2</sub>O<sub>4</sub> multilayer films react with amorphous ice clusters precovering the Au(111) surface and that the maximum amount of oxygen produced is about 0.5 ML.<sup>6,7</sup> This independence on the dosing sequence indicates that the Au surface plays little role in forming the initial intermediates that lead to oxygen formation and these are formed at the interface between N<sub>2</sub>O<sub>4</sub> and amorphous ice.

Other products in addition to O<sub>2</sub> were liberated into the gas phase during heating in TPD after H<sub>2</sub>O was exposed on an NO<sub>2</sub> precovered surface. For 2 ML H<sub>2</sub>O exposed on a 7.5 ML NO<sub>2</sub> precovered Au(111) surface at 86 K, Figure 6 shows that signals in the QMS during TPD were observed at  $m/e = 63, 47, 31, 46, 30, 18$ , and 32. These masses ostensibly monitor HNO<sub>3</sub>, HONO, HNO, NO<sub>2</sub>, NO, H<sub>2</sub>O, and O<sub>2</sub>, respectively. No evidence was observed in TPD for other possible reduction products such as H<sub>2</sub>, N<sub>2</sub>, NH<sub>3</sub>, N<sub>2</sub>O, and NH<sub>2</sub>NH<sub>2</sub>. We propose that HONO and HNO<sub>3</sub> are produced from these coadsorbed layers under UHV conditions below 145 K. The gas-phase HNO<sub>3</sub> mass spectrum shows a parent peak ( $m/e = 63$ ) that is only 1% in the mass spectrum cracking pattern, and HNO<sub>3</sub> does not produce HONO as an ion fragment.<sup>25</sup> It is uncertain whether HNO is a reaction product because the HONO mass spectrum is unknown and HNO could be a cracking fragment of HONO. In contrast to the oxygen formation pathway, acid formation reactions occur regardless of the NO<sub>2</sub> exposures, dosing sequence, or crystallinity of H<sub>2</sub>O in the coadsorbed layer.

The reactions during TPD depicted in Figure 6 are very complicated, but we tentatively assign the peaks in the low-

temperature range as follows. The peak at 161 K in H<sub>2</sub>O TPD is assigned to unreacted water because the desorption temperature is the same as that of multilayer H<sub>2</sub>O. The other three H<sub>2</sub>O desorption peaks at 174, 209, and 222 K arise either from interactions of H<sub>2</sub>O with adsorbed N<sub>2</sub>O<sub>4</sub> or from cracking of higher molecular weight products. Since the gas-phase N<sub>2</sub>O<sub>4</sub> mass spectrum does not give a fragment ion of  $m/e = 32$ , the peak at 143 K in O<sub>2</sub> TPD must be assigned to cracking from HNO<sub>3</sub> or HONO (or possibly some other unknown species). The O<sub>2</sub> peaks at 174, 209, and 222 K also arise from cracking of the products. In NO TPD, the peaks at 143, 174, and 222 K can be assigned to cracking from N<sub>2</sub>O<sub>4</sub>, HNO<sub>3</sub>, and other products. The long “tailing” of the NO desorption trace with a peak at 350–430 K is unusual and is likely to indicate that the decomposition of intermediates that finally produce oxygen adatoms on Au(111) cause reaction-rate-limited NO desorption over a wide temperature range. In NO<sub>2</sub> TPD, the peak at 143 K is mainly due to cracking from unreacted N<sub>2</sub>O<sub>4</sub> and the two higher desorption NO<sub>2</sub> peaks at 174 and 222 K arise from cracking of other products. In addition, the NO<sub>2</sub> TPD spectra also have a desorption profile that extends to quite high temperatures, including a peak at 350–430 K. This high-temperature NO<sub>2</sub> desorption is also reaction-rate limited<sup>7</sup> and is similarly produced from the decomposition of intermediates that finally generate oxygen adatoms on Au(111).

In other studies, we found that the oxygen formation reaction was highly dependent on the crystallinity of the ice when N<sub>2</sub>O<sub>4</sub> reacts with ice films on Au(111).<sup>6,7</sup> Figure 7a shows that this phenomena was also observed in the experiments in which H<sub>2</sub>O was exposed on N<sub>2</sub>O<sub>4</sub> films. Figure 7a, trace iii, shows that a substantial amount of O<sub>2</sub> was produced in TPD when 7.5 ML NO<sub>2</sub> (pure N<sub>2</sub>O<sub>4</sub>) was predosed on a Au(111) followed by dosing 1 ML H<sub>2</sub>O at 86 K. In Figure 7a, trace ii, a predosed 7.5 ML NO<sub>2</sub> film at 86 K was annealed to 115 K for 30 s and then 1 ML H<sub>2</sub>O was dosed on the film at 86 K. Under the conditions of Figure 7a, trace ii, about the same amount of O<sub>2</sub> was produced as that in Figure 7a, trace iii. Consistently, IRAS shows in Figure 2 that the NO<sub>2</sub> multilayer formed on Au(111) at 86 K is pure N<sub>2</sub>O<sub>4</sub> and subsequently annealing to 115 K does not change the chemical state of N<sub>2</sub>O<sub>4</sub>. In contrast, Figure 7a, trace i, shows that no O<sub>2</sub> was produced in TPD when a 7.5 ML NO<sub>2</sub> film was formed on Au(111) at 113 K and followed by dosing 1 ML H<sub>2</sub>O on the Au(111) at 113 K. This result clearly demonstrates that the crystallinity of the deposited ice clusters is a crucial factor for oxygen formation.

Previous IRAS studies showed that amorphous ice was formed when H<sub>2</sub>O was dosed on Au(111) at 86 K,<sup>7</sup> and this amorphous ice had non-hydrogen-bonded “free OH” groups.<sup>23,26</sup> These “free OH” groups were shown to have strong reactivity for oxygen formation when N<sub>2</sub>O<sub>4</sub> reacts with preadsorbed ice films, and “free OH” groups also show greater reactivity in other reactions compared to fully hydrogen-bonded crystalline ice.<sup>23,26,27</sup> Annealing amorphous ice to 115 K or dosing H<sub>2</sub>O at the same temperature produces crystalline ice and a loss in reactivity for oxygen formation since all of the “free OH” groups disappear because of crystallization that forms fully hydrogen-bonded ice species.<sup>7,23,26</sup> We propose that the strong hydrogen bonding between N<sub>2</sub>O<sub>4</sub> and the highly polar “free OH” groups on the amorphous ice surface plays a crucial role in breaking the N–N bond (where D(O<sub>2</sub>N–NO<sub>2</sub>) = 53 kJ/mol<sup>8</sup>) and stabilizing polar products and intermediates such as ONO–NO<sub>2</sub> and NO<sup>+</sup>NO<sub>3</sub><sup>–</sup>.

The reactivity of two other forms of nitrogen oxides, chelating chemisorbed NO<sub>2</sub> species and a pure monolayer of N<sub>2</sub>O<sub>3</sub>, with

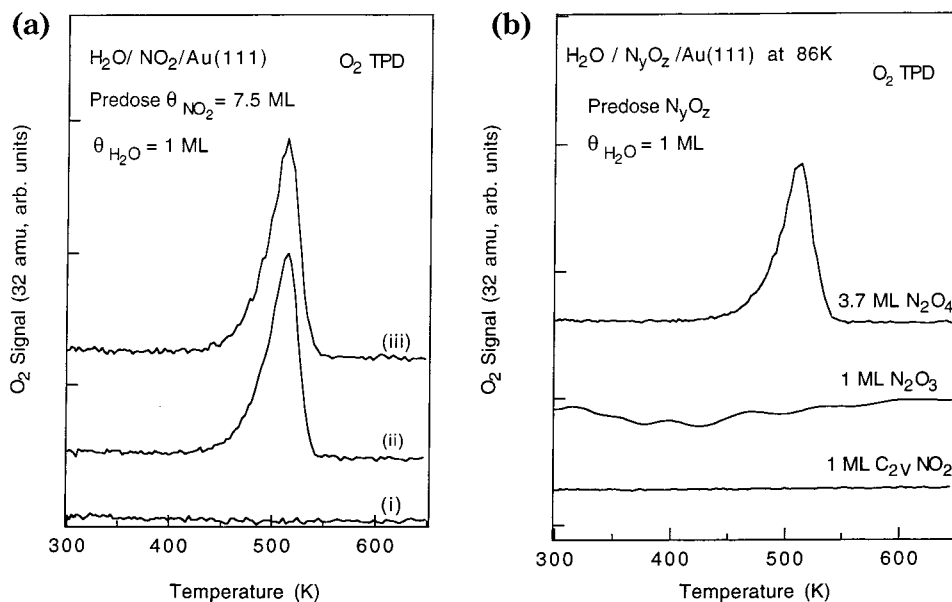


**Figure 7.** (a) O<sub>2</sub> TPD spectra probing requirements for generating surface oxygen: (i) 7.5 ML NO<sub>2</sub> predosed on Au(111) at 113 K followed by 1 ML H<sub>2</sub>O exposure at the same temperature; (ii) 7.5 ML NO<sub>2</sub> predosed on Au(111) at 86 K, then annealed to 115 K for 30 s, followed by dosing 1 ML H<sub>2</sub>O on the film at 86 K; (iii) 7.5 ML NO<sub>2</sub> predosed on Au(111) at 86 K followed by 1 ML H<sub>2</sub>O exposure at the same temperature. (b) O<sub>2</sub> TPD spectra probing the extent of oxygen formation on Au(111) for the reaction of amorphous ice clusters formed by 1 ML H<sub>2</sub>O exposures on preadsorbed films of (bottom) chelating NO<sub>2</sub> monolayer, (middle) N<sub>2</sub>O<sub>3</sub> monolayer, and (top) N<sub>2</sub>O<sub>4</sub> multilayer.

postdosed amorphous ice clusters on Au(111) at 86 K was also studied by TPD. The O<sub>2</sub> TPD spectra in Figure 7b show that no O<sub>2</sub> was produced either in reactions between chelating NO<sub>2</sub> or pure N<sub>2</sub>O<sub>3</sub> and amorphous ice. Therefore, only N<sub>2</sub>O<sub>4</sub> can react efficiently with amorphous ice to eventually oxidize the Au surface, and coadsorbed N<sub>2</sub>O<sub>3</sub> and chelating NO<sub>2</sub> block the interaction of “free OH” groups with N<sub>2</sub>O<sub>4</sub> to inhibit oxygen formation at low NO<sub>2</sub> exposures.

Comparing these results with our previous studies of N<sub>2</sub>O<sub>4</sub> reacting with preadsorbed amorphous ice films,<sup>7</sup> we find exactly the same results—acid formation and oxygen formation occur via two separate reaction pathways proceeding under different conditions. Acid-forming reactions are sensitive to neither the NO<sub>2</sub> exposure nor the crystallinity of the ice, but oxygen formation occurs only when amorphous ice is available and NO<sub>2</sub> exposure is in the multilayer range (to form pure N<sub>2</sub>O<sub>4</sub>). This demonstrates that the same oxygen formation mechanism is operating independent of the dosing sequence of NO<sub>2</sub> and H<sub>2</sub>O. We further proved in this study that N<sub>2</sub>O<sub>4</sub> is the only nitrogen oxide (of those investigated) that can (ultimately) produce oxygen by reacting with amorphous ice. This represents strong support for our proposed mechanism in which N<sub>2</sub>O<sub>4</sub> first isomerizes and forms NO<sup>+</sup>NO<sub>3</sub><sup>−</sup>, which finally decomposes at higher temperatures to form atomic oxygen on Au(111) during TPD.

Finally, the whole area of how N<sub>x</sub>O<sub>y</sub> interacts with water is important in the atmosphere. These studies reveal new information about fundamental interactions between N<sub>x</sub>O<sub>y</sub> and water (ice), for example, extending previous fundamental studies of N<sub>2</sub>O<sub>5</sub> and ice.<sup>28–30</sup>

#### 4. Conclusions

IRAS confirms the bonding geometries of NO<sub>2</sub>, N<sub>2</sub>O<sub>3</sub>, and N<sub>2</sub>O<sub>4</sub> adlayers on Au(111) deduced in previous HREELS studies. NO<sub>2</sub> exposures on Au(111) at 185 K produce a pure monolayer of chemisorbed, O,O′-chelating NO<sub>2</sub> with C<sub>2v</sub> symmetry. Exposing this chemisorbed NO<sub>2</sub> monolayer on Au(111) at 120 K to gas-phase NO leads to a monolayer of

adsorbed N<sub>2</sub>O<sub>3</sub> that is bonded to the surface through one oxygen and has C<sub>s</sub> symmetry. This conclusion about the monodentate bonding of N<sub>2</sub>O<sub>3</sub> clarifies the ambiguity that was left in the previous HREELS determination. Large NO<sub>2</sub> exposures on Au(111) at 86 K produce crystalline N<sub>2</sub>O<sub>4</sub> multilayers with a preferential orientation of the N–N bond perpendicular to the Au(111) surface.

Two reaction paths are found when preadsorbed layers of nitrogen oxides (NO<sub>2</sub>, N<sub>2</sub>O<sub>3</sub>, and N<sub>2</sub>O<sub>4</sub>) on Au(111) react with ice clusters formed by postdosing H<sub>2</sub>O on these surfaces at low temperatures. One path is associated with HONO and HNO<sub>3</sub> formation. This reaction channel proceeds regardless of the water exposure temperature (which controls the crystallinity and concentration of “free OH” groups of the ice clusters formed) and the size of the NO<sub>2</sub> exposures. The other reaction channel forms oxygen adatoms on the Au(111) surface during heating, and this pathway occurs only at the interface between amorphous ice clusters and N<sub>2</sub>O<sub>4</sub> in films deposited on Au(111). Conditions that form crystalline ice strongly inhibit this reaction. Also, two other adsorbed nitrogen oxides species, i.e., chelating NO<sub>2</sub> and N<sub>2</sub>O<sub>3</sub>, that are normally observed following NO<sub>2</sub> exposures on Au(111) at 86 K cannot react with amorphous ice to form oxygen on Au(111). These results are consistent with those of our previous studies of nitrogen oxides from NO<sub>2</sub> exposures reacting with amorphous ice films predeposited on Au(111). These observations support our proposed mechanism for the formation of oxygen adatoms on Au(111) in which nitrite—N<sub>2</sub>O<sub>4</sub>, a reactive precursor, is formed by interactions between “free OH” groups of amorphous ice and N<sub>2</sub>O<sub>4</sub> and then this species is converted to nitrosonium nitrate(NO<sup>+</sup>NO<sub>3</sub><sup>−</sup>), which produces oxygen adatoms on the surface following thermal decomposition.

These facile reactions between N<sub>x</sub>O<sub>y</sub> and H<sub>2</sub>O, along with the new structure–reactivity relationships established, are important to chemical foundations for a number of technologies, ranging from energetic materials to atmospheric chemistry.

**Acknowledgment.** This work was supported by the Army Research Office.

## References and Notes

- (1) Cotton, F. A.; Wilkinson, G. *Advanced Inorganic Chemistry*; Wiley-Interscience: New York, 1988.
- (2) Hisatsune, I. C.; Devlin, J. P.; Wada, Y. *J. Chem. Phys.* **1960**, *33*, 714.
- (3) Hitchman, M. A.; Rowbottom, G. L. *Coord. Chem. Rev.* **1982**, *42*, 55.
- (4) Koel, B. E.; Bartram, M. E. *J. Vac. Sci. Technol.* **1988**, *A6*, 782.
- (5) Koel, B. E. *Chemically Modified Oxide Surfaces*; Leyden, D. E., Collins, W. T., Eds.; Gordon and Breach Science Publishers: New York, 1989.
- (6) Wang, J.; Voss, M. R.; Busse, H.; Koel, B. E. *J. Phys. Chem.* **1998**, *B102*, 4693.
- (7) Wang, J.; Koel, B. E. *Surf. Sci.*, submitted.
- (8) Bartram, M. E.; Koel, B. E. *Surf. Sci.* **1989**, *213*, 137.
- (9) Wickham, D. T.; Banse, B. A.; Koel, B. E. *Catal. Lett.* **1990**, *6*, 163.
- (10) Xu, C.; Koel, B. E. *Surf. Sci.* **1993**, *292*, L803.
- (11) Wager, F. T.; Moylan, T. E. *Surf. Sci.* **1987**, *182*, 125.
- (12) Bartram, M. E.; Windham, R. G.; Koel, B. E. *Surf. Sci.* **1987**, *57*, 184.
- (13) Arakawa, E. T.; Nielsen, A. H. *J. Mol. Spectrosc.* **1958**, *2*, 413.
- (14) Goodgame, D. M. L.; Hitchman, M. A. *Inorg. Chem.* **1965**, *4*, 721.
- (15) Sjoval, P.; So, S. K.; Kasemo, B.; Franchy, R.; Ho, W. *Chem. Phys. Lett.* **1990**, *171*, 125.
- (16) Koch, T. G.; Horn, A. B.; Chesters, M. A.; McCoustra, M. R. S.; Sodeau, J. R. *J. Phys. Chem.* **1995**, *99*, 8362.
- (17) Nakamoto, K. *Infrared and Raman Spectra of Inorganic and Coordination Compounds*; Wiley: New York, 1986.
- (18) Bibart, C. H.; Ewing, G. E. *J. Chem. Phys.* **1974**, *61*, 1293.
- (19) Somorjai, G. A. *Interoduction to Surface Chemistry and Catalysis*; John Wiley & Sons Inc.: New York, 1994.
- (20) Kay, B. D.; Lykke, K. R.; Creighton, J. R.; Ward, S. J. *J. Chem. Phys.* **1989**, *91*, 5120.
- (21) Parker, D. H.; Koel, B. E. *J. Vac. Sci. Technol.* **1990**, *A8* (3), 2585.
- (22) Saliba, N.; Parker, D. H.; Koel, B. E. *Surf. Sci.*, in press.
- (23) Schaff, J. E.; Roberts, J. T. *J. Phys. Chem.* **1994**, *98*, 6900.
- (24) Buch, V.; Devlin, J. P. *J. Chem. Phys.* **1991**, *94*, 4091.
- (25) Dohl-oelze, R.; Brown, C. C.; Stuve, E. M. *Surf. Sci.* **1989**, *210*, 339.
- (26) Rowland, B.; Fisher, M.; Devlin, J. P. *J. Phys. Chem.* **1993**, *97*, 2485.
- (27) Gertner, B. J.; Hynes, J. T. *Science* **1996**, *271*, 1563.
- (28) Tolbert, M. A.; Rossi, M. J.; Golden, D. M. *Science* **1988**, *240*, 1018.
- (29) Chu, L. T.; Leu, M. T.; Keyser, L. F. *J. Phys. Chem.* **1993**, *97*, 12798.
- (30) Finlayson-Pitts, B. J. *Atmospheric Chemistry: fundamentals and experimental techniques*; Wiley: New York, 1986.